Multi-time Scale Optimal Dispatch of Railway FTPSS Based on Model Predictive Control

Minwu Chen, *Member, IEEE*, Zhe Cheng, Yuanli Liu, Yilin Cheng, and Zhongbei Tian

***Abstract*—The flexible traction power supply system (FTPSS) integrates back-to-back converter, hybrid energy storage system (HESS) and PV generation system will be an important part of the smart railway. The FTPSS not only cancels the neutral zone, but also facilitates the utilization of regenerative braking (RB) and renewable energy, but the random fluctuation of PV and the sudden change of traction load will exert influence on the safe and efficient operation of the FTPSS. To improve the benefits of FTPSS, and compensate the imbalance between supply and demand in short-term operation, a multi-time scale optimal dispatch method is proposed for flexible railway energy management (FREM), which integrate day-ahead dispatch and intra-day feedback correction. During the day-ahead dispatch, the minimizing operating costs problem is formulated as a mixed linear programming model by coordination between HESS, RB and PV output. For intra-day energy adjustment dispatch, a rolling optimization based on model predictive control combined with feedback correction method is proposed, with aim of minimum operation deviation of FTPSS for thanks to adjusting the HESS dispatch plan drew up at day-ahead. Finally, the effectiveness of the proposed FREM control strategy is verified by the detailed real case study of a railway line in China.**

***Index Terms*—Flexible traction power supply system Flexible railway energy management, hybrid energy storage, optimal operation, model predictive control.**

I. Introduction

In the conventional 27.5kV AC traction power supply system (TPSS), the neutral zone (NZ) is adopted to maintain all power supply sections electrically isolated so as to prevent the risk of mixing out-of-phase supplies, which not only affect the driving speed , cause a series of power-quality (PQ) problems[1], [2], but also becomes an obstacle for utilization of regenerative braking (RB) energy flow between train and substation. In order to solve these issues, a novel converter-based AC electrified railway flexible traction power supply system (FTPSS) is proposed [3]–[6], which not only achieve continuous power supply, but also provides the interface for the integration of PV and energy storage system. In [7], the additional converters connected to both side of NZs are outlined to allow exchange power between adjacent power supply interval. The detailed structure and coordinated control strategy of multi-converter of FTPSS is proposed in [8]–[10], more importantly, the PQ problems in conventional TPSS are solved. Reference [11] uses an improved PQ decomposition algorithm to analyze the system power flow, and illustrates the stable operating characteristics of the system under different operating conditions. [12] presents a neural network-based fault diagnosis method and system reconfiguration strategy of FTPSS to enhance the reliability and robustness of power supply in railway. Aforementioned studies and many other studies not referred here have proved that the FTPSS has practical application capability and development prospects, but the economical operation is seldom studied in existing literature. The interconnection and controllable of power flow characteristics of FTPSS can reduce the capacity of traction substation and improve energy utilization efficiency. With a integration of PV and energy storage into railway, the traction substation with power converters supplying could become more beneficial than conventional TPSS where power is supplied via a transformer [13]. It makes the current railway integration into smart grid possible considering economic criteria [14]. As a result, the development of flexible railway energy management (FREM) is necessary.

Based on the MERLIN Project, a railway energy management system (REM-S) concept with a "centralized-decentralized" architecture is proposed in [15]. By coordinating loads, regeneration, storage, and distributed-RES to realize daily global energy management and local management of minute-level and real time. Based on the REM-S framework, reference [16], [17] developed the REM-S software suite, and conducted offline and online tests on the DC railway in Malaga, Spain, respectively, verifying the effectiveness and reliability of the software suite. It offers the inspiration of applying the multi-time scale energy management to TPSS. [18] proposed an optimal scheduling approach of substation integrated RES, RB and HESS using a scenario reduction technology to account for uncertainty in renewable energy, the RES output is transformed into the deterministic scenario. However, the result of optimal scheduling is based on several special scenarios, the generation of the optimal scenario depends on the distribution probability of the initial scene. The scenario reduction algorithms to improve the calculation speed will lead to the loss of uncertainty information inevitably. In [19], railway station energy management (RSEM) architecture composed a detailed

This work was supported by the National Natural Science Foundation of China under Grant 51877182. (*Corresponding author: Zhe Cheng.*)

M. Chen, Z. Cheng, Y. Liu. and Y. Cheng are with the School of Electrical Engineering, Southwest Jiaotong University, Chengdu, Sichuan, 611756, China. (e-mail: chenminwu@home.swjtu.edu.cn; chengzhe@my.swjtu.edu.cn; 20130020@my.swjtu.edu.cn; q445772890@qq.com)

Z. Tian is with the Birmingham Centre for Railway Research and Education, School of Engineering, University of Birmingham, Birmingham B15 2TT, UK(e-mail: z.tian@bham.ac.uk).

mathematical model of the train considering the passengers numbers was established ,while the influence of the initial state of charge (SOC) of BESS on optimization result was studied. Unfortunately, the constraints of power supply and demand balance are required to be satisfied in each retained scenario. However, at the stage of intra-day operation, the balance constraints are not satisfied in all scenarios, as a result of the forecast errors of PV output and traction load. If the operation scheme is carried out based on several special scenarios, the power fluctuations of the utility grid will be presented. Calvillo et al. [20] investigated the joint coordination of distributed energy resources and electric urban transport systems, and the potentials of cost savings were also outlined. Two cases of railway connected to power grid were studied in [21] to reduce electricity and transportation costs, the optimal hourly dispatch of the battery storage system was solved by using time-space network model. There are much similar literature committed to the optimal operation of TPSS based on accurate prediction or specific scenarios of RES and traction load. However, due to the random factors of PV and traction load, forecast error between the actual value and prediction is neglected in those studies.

The static optimal dispatch methods have been investigated [18]–[20], in an optimization cycle, all the optimal solution sequences of a period in the future (e.g. one day) are obtained and delivered. However, as the prediction time horizon increases, the prediction accuracy decreases, and the optimal dispatch sequences cannot be directly applied to the actual system. Model predictive control (MPC) has received extensive attention as a dynamic method for power system optimization operation after RES access. Reference [22] proposed an energy flow control strategy based on MPC to suppress the operation point deviated from the point set one day in advance caused by fluctuating RES. There are also some interesting works on combined cooling, heating and power (CCHP) system and microgrid based on MPC [23]–[27]. The MPC for train management of a subway line is designed in [28], and the delay of subway is reduced after optimization, but the system cost function does not take the electricity bill into account. References [29]–[31] developed a hierarchical structure including a lower hierarchical level to optimize on-route trains energy consumption and higher hierarchical level to optimize traction substation energy flows. In HHL, the optimal economic cost problem is solved by MPC on the prediction horizon *N*. However, no strategy of feedback control is considered. Aforementioned studies and many other studies not referred here gave approaches to energy management in conventional TPSS from different perspectives, which present the potential of FREM in FTPSS. Compared with conventional railway energy management, how to maintain optimal operation of railway system while control HESS and manage energy flow in short-term operation to reduce the negative impacts of uncertainty in RES and dramatic stochastic volatility in traction load become challenges for application of FREM.

Accordingly, this paper aims at providing an insight into these problems. The highlights of this paper can be outlined as follows: i) a novel converter-based FTPSS that integrate PV and HESS is considered, achieving line connectivity and continuous power supply. The substations implement different electricity tariff standards. ii) A multi-time scale optimal dispatch model is proposed, the proposed approach promotes the economic operation of railway and reduces running cost. iii) the prediction error caused by the random fluctuation of PV and volatile of traction load is taken into account, the proposed rolling optimization strategy based on MPC has a good performance on correcting the intra-day running deviation. The case study show that the computing time of the proposed method for each interval is acceptable for actual operation.

The paper is organized as follows. System description of FTPSS and FREM control strategy is presented in Section II. The concept and mathematical model of day-ahead optimal dispatch are elaborated in Section III. The intra-day control strategy is described in detail in Section IV together with the corresponding case study presented in Section V. Finally, conclusions are given in Section VI.

II. System Description

In conventional TPSS, traction transformer is usually connected to two-phase of three-phase grid. The second side is connected to two power supply arms via feeder, and the neutral section is set in the middle. This type of wiring causes PQ problems such as unbalance voltage, and high transformer capacity and high demand charge. Moreover, it is not conducive to the access of RES and HESS. To solve those problems, a novel FTPSS is proposed, the structure of FTPSS is illustrated in Fig. 1, which is developed from the converter-based TPSS proposed in [8], [10], [13]. The FTPSS is composed of power grid, three-phase to single-phase converter, HESS, PV generation and high-speed trains (HSTs). Because the frequency, phase and amplitude of supplied voltage are controlled automatically, and intermediate DC-link of converter, the FTPSS not only eliminates the neutral section of the substation and the post station, achieves link of different substations but also facilitates the absorption of PV and energy storage access. The FREM system manages the coordinated operation of traction substations taking power source-load-storage into account. In order to reduce the operating costs of railway management department, and according to the characteristics that the forecast error of distributed renewable energy decreases with the shortening of prediction time scale [32], this paper divided the optimal scheduling of FREM into day-ahead economic dispatch stage and intra-day rolling feedback correction stage, and optimal dispatch framework of FREM under multi-time scale as shown in Fig. 2.

As shown in Fig. 2, in the day-ahead dispatch stage, the FREM is based on the predicted power output of PV, railway traction load and RB power profile, considers the constraints of storage capacity and the system dynamic comprehensively. An optimal economy scheduling model is formulated, in which the connection schemes of traction substations access to different power grid were also taken into account. So the optimal charging or discharging power of each energy storage device, and the exchange power of the inlet-line connecting substation and utility grid is determined. The basic dispatch plan for each time interval (Δt) of the next day is draw up and released in advance. During the intra-day dispatching stage, the charge and discharge state of the energy storage equipment will be managed in accordance with the day-ahead dispatch plan.

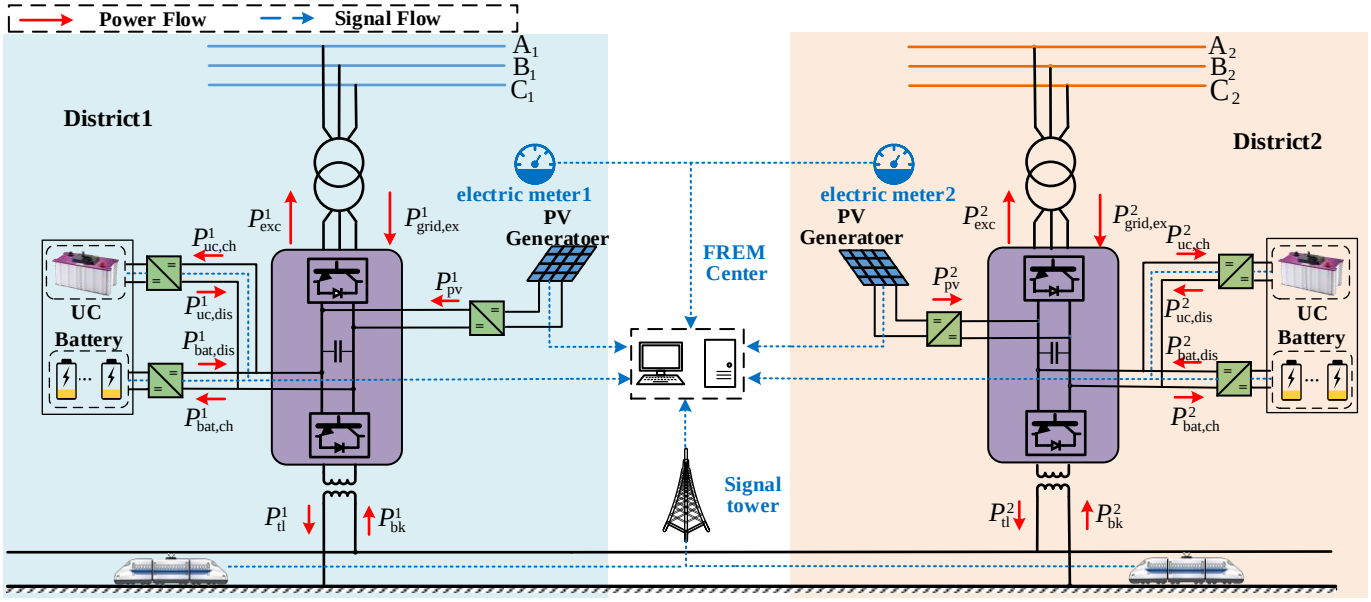

Fig. 1. Structure of Flexible Traction power supply system

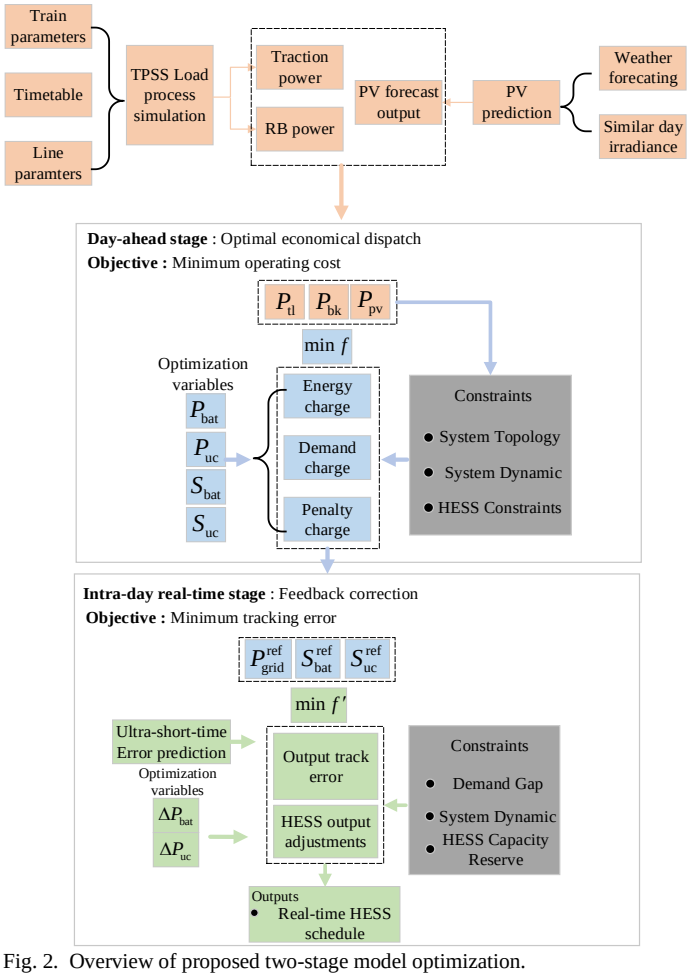

Fig. 2. Overview of proposed two-stage model optimization.

During the intra-day stage, in order to eliminate the actual operation deviation of the day caused by forecast error, the intra-day feedback correction is performed by rolling optimization based on MPC with a cycle of Δt^*. The time interval Δt^* is smaller than Δt. In the rolling process, the ultra-short-term RES and traction load error forecast and

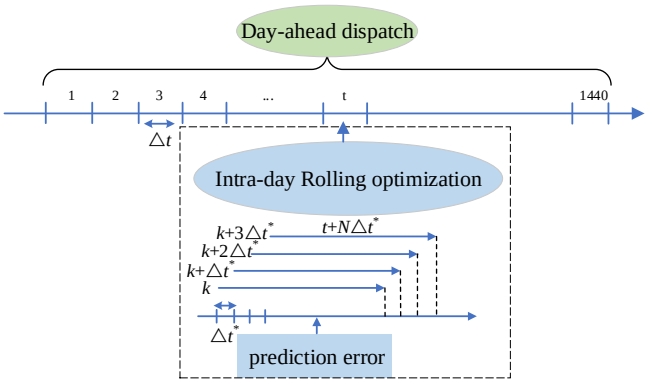

Fig. 3. Optimal dispatch framework of FTPSS under multi-time scale.

optimization is implemented in each time step. By solving the objective function, all correction plans of HESS within the time window are obtained to satisfy the supply and demand balance constraints of substations and HSTs. At the beginning of the k time step, the optimization problem is solved over the prediction horizon (from the k+1 to k+N time interval), and only the correction plans of next time period (k+1) is conducted. When the next dispatch time comes, the time horizon moves forward one interval as shown in Fig. 3, the above process is repeated using the actual system running state sampled from the HESS and traction side. By this control approach, feedback is introduced into an intra-day correction. The optimization keeps account of future time intervals, so that the control remains optimal [24]. It should be noted that in the intra-day stage, the system might violate operational constraints when the PV has increasingly excessive output and traction load operation diagram change. It is necessary to conduct a new dispatch for all the components in the day-ahead stage.

III. Day-ahead Optimal Dispatch

In the day-ahead optimal dispatch part, forecast and

optimization are implemented in a full day time scale. According to [33], the day-ahead forecast power of PV is generated by the weather forecast and similar day historical irradiance data. The generation of day-ahead traction load data is based on load process simulation of FTPSS [34]. The day-ahead dispatch is to solve an optimal economical operation problem, by which the scheduling of HESS all of a day, the power purchase and power fed back to the grid is determined. As a bulk industrial consumer of power grid in China, electrified railway is charged based on two-part tariff which consists of exchanged electricity charge and demand charge. The exchanged electricity charge is associated with the energy consumption of TPSS supplied by the utility grid and corresponding energy price including fixed tariff or time-of-use (TOU) tariff. The demand charge is defined as the maximum average active power through traction transformer in a 15minutes time window during a month (in this study, one cycle is one day due to traction load and traction substation repeatedly running on a daily cycle). This part of cost is relevant to the process of traction load. In addition, punishment bill is charged for the RB power fed back to the utility grid [34]. Therefore the objective function can be expressed as:

$$\min C_{\mathrm{DAC}} = C_{\mathrm{EC}} + C_{\mathrm{DC}} + C_{\mathrm{PC}} \tag{1}$$

The first term of the objective function (1) accounts for the exchanged electricity charge (EC):

$$C_{\mathrm{EC}} = \sum_{i=1}^{N_{\mathrm{Dis}}} \left(\sum_{t=1}^{\mathrm{T}} \pi_{\mathrm{EC}}^{i,t} \cdot P_{\mathrm{grid,ex}}^{i,t} \cdot \Delta t \right) \qquad \forall i,t \tag{2}$$

The second term of the objective function (1) is the demand charge (DC), calculated as maximum average active power of traction substation every 15 minutes in a day multiplied by the demand unit price specified by the grid company.

$$C_{\mathrm{DC}} = \sum_{i=1}^{N_{\mathrm{Dis}}} \pi_{\mathrm{DC}}^{i,t} \cdot \max(P_{\mathrm{dm}}^{i,t}) \quad \forall i, t = 1,2,...,\mathrm{T}-14 \tag{3}$$

$$P_{\mathrm{dm}}^{i,t'} = \sum_{t}^{t+14} P_{\mathrm{grid,ex}}^{i,t} / 15 \ \forall i, t = 1,16,...,\mathrm{T}-14, t' = T/15 \tag{4}$$

Due to the RB power fed back to the power system contains a large number of harmonic components and negative sequence components, bring potential threats to the utility grid. Therefore, punishment charge (PC) is charged for the traction power fed back to the utility grid:

$$C_{\mathrm{PC}} = \sum_{i=1}^{N_{\mathrm{Dis}}} \left(\sum_{t=1}^{\mathrm{T}} \pi_{\mathrm{PC}}^{i,t} \cdot P_{\mathrm{exc}}^{i,t} \cdot \Delta t \right) \qquad \forall i,t \tag{5}$$

where Δt is a discretization time interval, T represents the number of the time step in one day and N_{Dis} is the number of traction substations distributed in different areas; $\pi_{\mathrm{EC}}^{i,t}$ (¥/MW), $P_{\mathrm{grid,ex}}^{i,t}$ (MW) denotes the purchased electricity price and active power consumed by inlet-line of traction substation i in time interval Δt ; π_{DC} (¥/MW) is demand electricity price of industrial consumer i; $P_{\mathrm{dm}}^{i,t}$ (MW) is load demand of traction substation in district i which is calculated by average active power consumed in continuous 15 minutes time window. $\pi_{\mathrm{PC}}^{i,t}$ (¥/MW)and $P_{\mathrm{exc}}^{i,t}$ (MW) refer to the punishment price and the excessive power returned to power grid of district i respectively.

The auxiliary variable P_{peak}^{i} is introduced to solve the nonlinear problem caused by (3). By the constraint (7), P_{peak}^{i} is not less than any value of power sequence $P_{\mathrm{dm}}^{i,t'}$, and the objective function aims to find the minimum demand, so P_{peak}^{i} does not exceed the maximum value of $P_{\mathrm{dm}}^{i,t'}$. In this way, the non-convex constraints of the original equation (3) are transformed into convex linear constraints of (6) and (7).

$$C_{\mathrm{DC}} = \pi_{\mathrm{DC}}^{i} \cdot P_{\mathrm{peak}}^{i} \qquad \forall i \tag{6}$$

$$P_{\mathrm{peak}}^{i} \geq P_{\mathrm{dm}}^{i,t'} \qquad \forall i, t' = 1,2,...,\mathrm{T}/15 \tag{7}$$

where P_{peak}^{i} is an auxiliary variable constrained by the maximum demand load of traction substation i.

It is worth noting that the decision variables in FREM are divided into two types. One is successive variables which are used to denote the state of energy or power of the traction substation components, including $P_{\mathrm{grid,ex}}^{i,t}$, $P_{\mathrm{exc}}^{i,t}$, $P_{\mathrm{bat,ch}}^{i,t}$, $P_{\mathrm{bat,dis}}^{i,t}$, $P_{\mathrm{uc,ch}}^{i,t}$, $P_{\mathrm{uc,dis}}^{i,t}$, $E_{\mathrm{bat}}^{i,t}$ and $E_{\mathrm{uc}}^{i,t}$. The other is binary variables which are used to indicate the switch status of HESS and power flow direction of inlet-line, including $b_{\mathrm{bat,ch}}^{i,t}$, $b_{\mathrm{bat,dis}}^{i,t}$, $b_{\mathrm{uc,ch}}^{i,t}$, $b_{\mathrm{uc,dis}}^{i,t}$, $b_{\mathrm{grid,ex}}^{i,t}$ and $b_{\mathrm{tl}}^{i,t}$.

As shown in (8), the active power balance of elements in the TPSS is presented. It indicates that the power consumption of traction load ($P_{\mathrm{tl}}^{i,t}$), excessive power fed back to grid ($P_{\mathrm{exc}}^{i,t}$), battery charging power ($b_{\mathrm{bat,ch}}^{i,t}$)and UC charging power ($P_{\mathrm{uc,ch}}^{i,t}$) should be equal to the active power absorbed from the utility grid ($P_{\mathrm{grid,ex}}^{i,t}$), the regenerative braking power fed back to traction substation($P_{\mathrm{bk}}^{i,t}$), battery discharging power($P_{\mathrm{bat,dis}}^{i,t}$), UC discharging power($P_{\mathrm{uc,dis}}^{i,t}$) and PV forecast output($P_{\mathrm{pv}}^{i,t}$).

$$\begin{aligned} &P_{\mathrm{grid,ex}}^{i,t} + P_{\mathrm{pv}}^{i,t} + P_{\mathrm{bat,dis}}^{i,t} + P_{\mathrm{uc,dis}}^{i,t} + P_{\mathrm{bk}}^{i,t} \\ &\quad = P_{\mathrm{tl}}^{i,t} + P_{\mathrm{bat,ch}}^{i,t} + P_{\mathrm{uc,ch}}^{i,t} + P_{\mathrm{exc}}^{i,t} \quad \forall i,t \end{aligned} \tag{8}$$

$$E_{\mathrm{bat}}^{i,t} = (1-\kappa_{\mathrm{bat}}) E_{\mathrm{bat}}^{i,t-1} + \eta_{\mathrm{bat}}^{\mathrm{ch}} P_{\mathrm{bat,ch}}^{i,t} \Delta t - P_{\mathrm{bat,dis}}^{i,t} \Delta t / \eta_{\mathrm{bat}}^{\mathrm{dis}} \quad \forall i,t \tag{9}$$

$$E_{\mathrm{uc}}^{i,t} = (1-\kappa_{\mathrm{uc}}) E_{\mathrm{uc}}^{i,t-1} + \eta_{\mathrm{uc}}^{\mathrm{ch}} P_{\mathrm{uc,ch}}^{i,t} \Delta t - P_{\mathrm{uc,dis}}^{i,t} \Delta t / \eta_{\mathrm{uc}}^{\mathrm{dis}} \quad \forall i,t \tag{10}$$

$$0 \leq P_{\mathrm{bat,ch}}^{i,t} \leq \min((\mathrm{S}_{\mathrm{bat}}^{\max} \cdot \mathrm{Cap}_{\mathrm{bat}} - E_{\mathrm{bat}}^{i,t}) / \eta_{\mathrm{bat}}^{\mathrm{ch}} \Delta t, \mathrm{R}_{\mathrm{bat}}) \forall i,t \tag{11}$$

$$0 \leq P_{\mathrm{bat,dis}}^{i,t} \leq \min((E_{\mathrm{bat}}^{i,t} - \mathrm{S}_{\mathrm{bat}}^{\min} \cdot \mathrm{Cap}_{\mathrm{bat}}) \eta_{\mathrm{bat}}^{\mathrm{dis}} / \Delta t, \mathrm{R}_{\mathrm{bat}}) \forall i,t \tag{12}$$

$$0 \leq P_{\mathrm{uc,ch}}^{i,t} \leq \min((\mathrm{S}_{\mathrm{uc}}^{\max} \cdot \mathrm{Cap}_{\mathrm{uc}} - E_{\mathrm{uc}}^{i,t}) / \eta_{\mathrm{uc}}^{\mathrm{ch}} \Delta t, \mathrm{R}_{\mathrm{uc}}) \forall i,t \tag{13}$$

$$0 \leq P_{\mathrm{uc,dis}}^{i,t} \leq \min((E_{\mathrm{uc}}^{i,t} - \mathrm{S}_{\mathrm{uc}}^{\min} \cdot \mathrm{Cap}_{\mathrm{uc}}) \eta_{\mathrm{uc}}^{\mathrm{dis}} / \Delta t, \mathrm{R}_{\mathrm{uc}}) \ \forall i,t \tag{14}$$

$$S_{\mathrm{bat}}^{\min} \cdot \mathrm{Cap}_{\mathrm{bat}} \leq E_{\mathrm{bat}}^{i,t} \leq S_{\mathrm{bat}}^{\max} \cdot \mathrm{Cap}_{\mathrm{bat}} \qquad \forall i,t \tag{15}$$

$$\mathrm{S}_{\mathrm{uc}}^{\min} \cdot \mathrm{Cap}_{\mathrm{uc}} \leq E_{\mathrm{uc}}^{i,t} \leq \mathrm{S}_{\mathrm{uc}}^{\max} \cdot \mathrm{Cap}_{\mathrm{uc}} \qquad \forall i,t \tag{16}$$

$$E_{\mathrm{bat}}^{i,t=1} = E_{\mathrm{bat}}^{i,t=\mathrm{end}} = \mathrm{S}_{\mathrm{bat}}^{\mathrm{initial}} \cdot \mathrm{Cap}_{\mathrm{bat}} \tag{17}$$

$$E_{\mathrm{uc}}^{i,t=1} = E_{\mathrm{uc}}^{i,t=\mathrm{end}} = \mathrm{S}_{\mathrm{uc}}^{\mathrm{initial}} \cdot \mathrm{Cap}_{\mathrm{uc}} \tag{18}$$

$$P_{\mathrm{bat,ch}}^{i,t} \leq b_{\mathrm{bat,ch}}^{i,t} \cdot \mathrm{R}_{\mathrm{bat}}, P_{\mathrm{bat,dis}}^{i,t} \leq b_{\mathrm{bat,dis}}^{i,t} \cdot \mathrm{R}_{\mathrm{bat}} \qquad \forall i,t \tag{19}$$

$$P_{\mathrm{uc,ch}}^{i,t} \leq b_{\mathrm{uc,ch}}^{i,t} \cdot \mathrm{R}_{\mathrm{bat}}, P_{\mathrm{uc,dis}}^{i,t} \leq b_{\mathrm{uc,dis}}^{i,t} \cdot \mathrm{R}_{\mathrm{uc}} \qquad \forall i,t \tag{20}$$

$$b_{\mathrm{bat,ch}}^{i,t} + b_{\mathrm{bat,dis}}^{i,t} \leq 1, b_{\mathrm{uc,ch}}^{i,t} + b_{\mathrm{uc,dis}}^{i,t} \leq 1 \qquad \forall i,t \tag{21}$$

where κ_{bat} and κ_{uc} are battery and UC self-discharging coefficient, $\eta_{\mathrm{bat}}^{\mathrm{ch}}, \eta_{\mathrm{bat}}^{\mathrm{dis}}$, $\eta_{\mathrm{uc}}^{\mathrm{ch}}$, $\eta_{\mathrm{uc}}^{\mathrm{dis}}$ are battery and UC efficiency of charging and discharging respectively. Equation (9) denotes that the energy stored in a battery at time t is equal to energy stored at time t-1 add (or minus) the amount of energy charged (or discharged) at interval Δt, and the effect of self-discharge and charging/discharging efficiency Δt is also considered. So as to the remaining capacity constraint of UC shown in (10). Equation (11) to (14) indicate that both the battery and UC power are restricted by rated power and available capacity per time interval. Equations (15) to (16) imply the SOC of energy

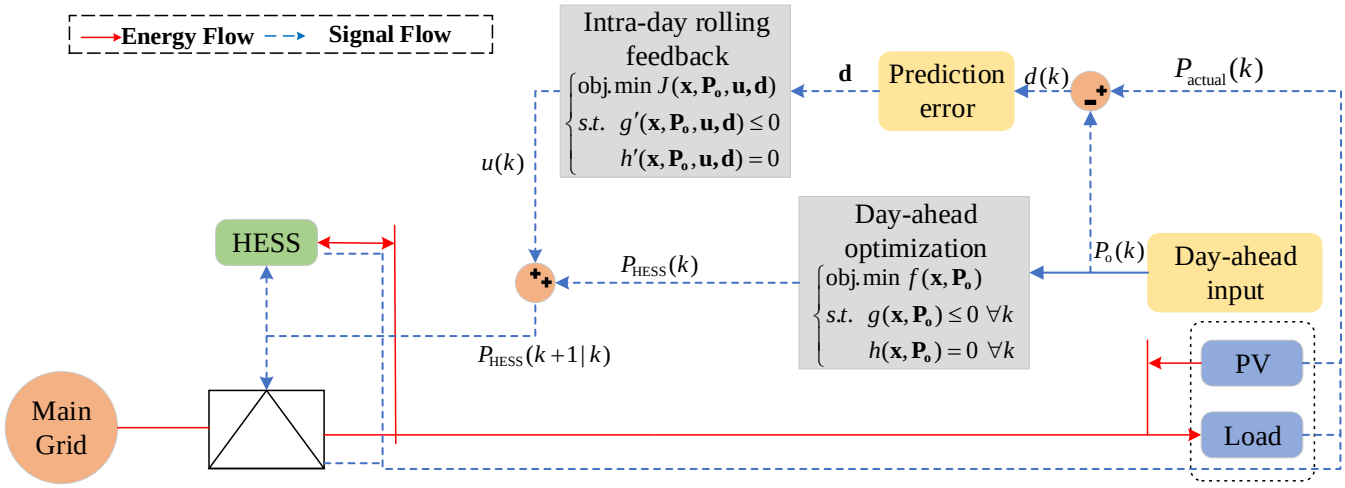

Fig. 4. Control block diagram of FREM

storage equipment cannot exceed the upper and lower restriction allowed singly, to avoid extra lifetime loss resulting from overcharge/overdischarge. Due to the daily repeated operation characteristics of FTPSS, the energy stored in HESS at the first time interval equal to that at end-time interval, as shown in (17) and (18). Last but not least, the charge state of HESS cannot exist simultaneously with the discharge state by applying constraints (19) to (21). Introduced binary variable $b_{\text{bat,ch}}^{i,t}$ is 1 indicate that battery is in charging status, and otherwise 0; In contrast, binary variable $b_{\text{bat,dis}}^{i,t}$ is 1 state that battery is in discharging status and otherwise 0. And it is same to UC.

$$P_{\text{grid,ex}}^{i,t} \le b_{\text{grid,ex}}^{i,t} \cdot S_{\text{grid,ex}}^{\max} \qquad \forall i,t \qquad (22)$$

$$P_{\text{exc}}^{i,t} \le (1-b_{\text{grid,ex}}^{i,t}) \cdot S_{\text{grid}}^{\max} \qquad \forall i,t \qquad (23)$$

$$P_{\text{tl}}^{i,t} \le b_{\text{tl}}^{i,t} \cdot S_{\text{tl}}^{\max} \qquad \forall i,t \qquad (24)$$

$$P_{\text{bk}}^{i,t} \le (1-b_{\text{tl}}^{i,t}) \cdot S_{\text{tl}}^{\max} \qquad \forall i,t \qquad (25)$$

The FTPSS must ensure that the traction load demand and the grid supply are balanced, and feed the regenerative braking power that cannot be absorbed by the HESS back to the grid, both the above situation will not take place at the same time interval. The auxiliary binary variables $b_{grid}^{i,t}$ and $b_{\text{tl}}^{i,t}$ are introduced to constrain the power flow direction of FTPSS. Equations (22) and (23) state that $b_{\text{grid}}^{i,t}$=1 if power flows to the DC-link through the grid-side converter, 0 if excess power fed back to grid, and both of them are constrained by the converter capacity ($S_{\text{grid}}^{\max}$). Equations (24) and (25) state that $b_{\text{tl}}^{i,t}$=1 if FTPSS supplies power to HSTs through traction-side converter, 0 if RB power is returned to substation, and both of them are constrained by the converter capacity ($S_{\text{tl}}^{\max}$).

IV. Intra-day Optimal Dispatch

MPC is a model-based closed-loop optimization control method. The kernel idea of the algorithm is a rolling time strategy. For simplicity, Use $x(k) \in R^w$ to represent system state variables at step k, such as exchange power from grid, SOC of HESS, and $\mathbf{x}=.\{x(k),x(k+1),...,x(k+N)\}$. For all the steps in the time horizon, vector $u(k) \in R^m$ represents the control variables, mainly the adjustment of the HESS, $\mathbf{u}=.\{u(k),u(k+1),...,u(k+N\text{-}1)\}$. $P_o(k) \in R^l$ is the parameters representing system demand, PV generation at time step k, $\mathbf{P_o}=\{P_o(k),P_o(k+1),...,P_o(k+N)\}$, and $d(k) \in R^n$ represent the prediction error vector, $\mathbf{d}=\{d(k),d(k+1|k),...,d(k+N\text{-}1)\}$. Fig. 4 shows the control block diagram of FREM, which is summarized below:

Step 1: At the current time k, based on the current state $x(k)$, predicting the future state of the system $\mathbf{x}$, taking into account current and future constraints, and solving the optimization problem to obtain the k+1, k+2, ...,k +N optimal control sequence $\mathbf{u}$ in the future;

Step 2: Apply the first control vector of the optimal control sequence $u(k)$ to the control system;

Step 3: At time of k+1, update system actual state of $x(k+1)$, Repeat the above steps.

In order to cope with the inlet-line power fluctuation of traction substation result from the uncertainty of RES and traction load, ensure that the inlet-line power tracking the planned value of day-ahead. And at the same time ,to ensure that the SOC of battery and UC in the intra-day scheduling follow the running curve set by day-ahead. The objective of intra-day optimal dispatch is to minimize error between power of inlet-line, SOC of HESS and plan draw up at day-ahead stage, and control adjustments of battery and UC are kept as small as possible. The goal function can be expressed as:

$$\begin{aligned}\min J_{\text{intra}} = &\sum_{p=1}^{N}(\omega_p(P_{\text{grid}}^{i,\text{ref}}(k+p\Delta t^*)-P_{\text{grid}}^{i,\text{int}}(k+p\Delta t^*|k))^2)\\ &+\omega_{\text{bat}}(SOC_{\text{bat}}^{i,\text{ref}}(k+p\Delta t^*)-SOC_{\text{bat}}^{i,\text{int}}(k+p\Delta t^*|k))^2\\ &+\omega_{\text{uc}}(SOC_{\text{uc}}^{i,\text{ref}}(k+p\Delta t^*)-SOC_{\text{uc}}^{i,\text{int}}(k+p\Delta t^*|k))^2)\\ &+\sum_{p=1}^{N}(\lambda_{\text{bat}}\Delta P_{bat}^{i}(k+p\Delta t^*|k)^2+\lambda_{\text{uc}}\Delta P_{\text{uc}}^{i}(k+p\Delta t^*|k)^2)\end{aligned} \qquad (26)$$

where $P_{\text{gird}}^{i,\text{ref}}(k+p\Delta t^*)$, $S_{\text{bat}}^{i,\text{ref}}(k+p\Delta t^*)$, $S_{\text{uc}}^{i,\text{ref}}(k+p\Delta t^*)$ are reference value of inlet-line power, SOC of battery and UC at time k+$p\Delta t$ respectively. $P_{\text{gird}}^{i,\text{int}}(k+p\Delta t^*|k)$, $S_{\text{bat}}^{i,\text{int}}(k+p\Delta t^*|k)$, $S_{\text{uc}}^{i,\text{int}}(k+p\Delta t^*|k)$ imply that the MPC controller forecast output of inlet-power and SOC of HESS at time k+$p\Delta t^*$. $P_{\text{grid}}^{i,\text{int}}(k+p\Delta t^*|k)>0$ means that power flow from the utility grid to traction substation, and < 0 mean that power flow in the opposite direction, $\Delta P^i(k+p\Delta t^*|k)$ indicate that output increment of battery and UC at time k+$p\Delta t^*$. ω_p, ω_{bat} and ω_{uc} are weight coefficients of tracking error of inlet-line power, SOC of battery and UC, respectively. λ_{bat}, λ_{uc} are the weight

coefficients of the MPC controller control increment. $p \in \mathbf{\Omega}=\{1,2,\ldots N\}$ represents the set of time steps in the prediction horizon.

The PV output and traction load are uncertain, considering their ultra-short-term prediction errors during intra-day, an intra-day revised power balance equation is established, as shown in (27):

$$\begin{aligned} &P_{\text{grid}}^{i,\text{int}}(k+p\Delta t^*\mid k)+P_{\text{pv}}^{i}(k)+\sum_{j=1}^{p}\Delta P_{\text{pv}}^{i}(k+j\Delta t^*\mid k)\\ &\quad=P_{\text{tl}}^{i}(k)+\sum_{j=1}^{p}\Delta P_{\text{tl}}^{i}(k+j\Delta t^*\mid k)\\ &\quad+P_{\text{bat}}^{i}(k)+\sum_{j=1}^{p}\Delta P_{\text{bat}}^{i}(k+j\Delta t^*\mid k)\\ &\quad+P_{\text{uc}}^{i}(k)+\sum_{j=1}^{p}\Delta P_{\text{uc}}^{i}(k+j\Delta t^*\mid k) \end{aligned} \tag{27}$$

where $P_{\text{pv}}^{i}(k)$, $P_{\text{bat}}^{i}(k)$, $P_{\text{uc}}^{i}(k)$ are PV output, power of battery and UC at time k respectively, can be measured by actual device of substation. $P_{\text{tl}}^{i}(k)$ presents the traction load, where positive values indicate the power supplied to the traction side, and negative values indicate power fed back to the DC-link. $\Delta P_{\text{pv}}^{i}(k+j\Delta t^*\mid k)$, $\Delta P_{\text{tl}}^{i}(k+j\Delta t^*\mid k)$ indicate that the ultra-short-time predicted power increments of traction load, PV in the future $(k+(j-1)\Delta t^*,\ k+j\Delta t^*]$ period, the PV forecast error ΔP_{pv}^{i} can be described by normal distribution [35]. The random fluctuation of train power is determined by line ramp slope, which can also be describe by normal distribution [36].

The constraints of HESS and converter can be corrected as (28) to (38),

$$\begin{aligned} E_{\text{bat}}^{i,\text{intra}}(k+p\Delta t^*\mid k)&=(1-\kappa_{bat})E_{\text{bat}}^{i,\text{intra}}(k+(p-1)\Delta t^*\mid k)\\ &\quad-\eta_{\text{bat}}P_{\text{bat}}^{i}(k+p\Delta t^*\mid k)\Delta t^* \quad p\in\mathbf{\Omega} \end{aligned} \tag{28}$$

$$\begin{aligned} E_{\text{uc}}^{i,\text{int}}(k+p\Delta t^*\mid k)&=(1-\kappa_{\text{uc}})E_{\text{uc}}^{i,\text{int}}(k+(p-1)\Delta t^*\mid k)\\ &\quad-\eta_{\text{uc}}P_{\text{uc}}^{i}(k+p\Delta t^*\mid k)\Delta t^* \quad p\in\mathbf{\Omega} \end{aligned} \tag{29}$$

$$\eta_{\text{bat}}=\begin{cases}\eta_{\text{bat}}^{\text{ch}} & \text{if } P_{\text{bat}}^{i}(k)\ge 0\\ \dfrac{1}{\eta_{\text{bat}}^{\text{dis}}} & \text{if } P_{\text{bat}}^{i}(k)<0\end{cases} \qquad \eta_{\text{UC}}=\begin{cases}\eta_{\text{uc}}^{\text{ch}} & \text{if } P_{\text{uc}}^{i}(k)\ge 0\\ \dfrac{1}{\eta_{\text{uc}}^{\text{dis}}} & \text{if } P_{\text{uc}}^{i}(k)<0\end{cases} \tag{30}$$

$$\text{S}_{\text{bat}}^{\min}\cdot\text{Cap}_{\text{bat}}\le E_{\text{bat}}^{i,\text{int}}(k+p\Delta t^*\mid k)\le \text{S}_{\text{bat}}^{\max}\cdot\text{Cap}_{\text{bat}}\ p\in\mathbf{\Omega} \tag{31}$$

$$\text{S}_{\text{uc}}^{\min}\cdot\text{Cap}_{\text{uc}}^{\text{rate}}\le E_{\text{uc}}^{i,\text{int}}(k+p\Delta t^*\mid k)\le \text{S}_{\text{uc}}^{\max}\cdot\text{Cap}_{\text{uc}}^{\text{rate}}\ p\in\mathbf{\Omega} \tag{32}$$

$$-\text{R}_{\text{bat}}\le P_{\text{bat}}^{i}(k)+\Delta P_{\text{bat}}^{i}(k+p\Delta t^*\mid k)\le \text{R}_{\text{bat}}\ p\in\mathbf{\Omega} \tag{33}$$

$$-\text{R}_{\text{uc}}\le P_{\text{uc}}^{i}(k)+\Delta P_{\text{uc}}^{i}(k+p\Delta t^*\mid k)\le \text{R}_{\text{uc}}\ p\in\mathbf{\Omega} \tag{34}$$

$$\Delta P_{\text{bat}}^{i,\min}\le\Delta P_{\text{bat}}^{i}(k+p\Delta t^*\mid k)\le\Delta P_{\text{bat}}^{i,\max}\quad p\in\mathbf{\Omega} \tag{35}$$

$$\Delta P_{\text{uc}}^{i,\min}\le\Delta P_{\text{uc}}^{i}(k+p\Delta t^*\mid k)\le\Delta P_{\text{uc}}^{i,\max}\quad p\in\mathbf{\Omega} \tag{36}$$

$$\left|P_{\text{grid}}^{i,\text{int}}(k+p\Delta t^*)\right|\le S_{\text{grid}}^{\max}\quad p\in\mathbf{\Omega} \tag{37}$$

$$\left|P_{\text{tl}}^{i,\text{int}}(k+p\Delta t^*)\right|\le S_{\text{tl}}^{\max}\quad p\in\mathbf{\Omega} \tag{38}$$

where $E_{\text{bat}}^{i,\text{int}}(k+p\Delta t^*\mid k)$ denote that at the time step k, the prediction of energy stored in battery at future $k+p\Delta t$ time, $E_{\text{uc}}^{i,\text{int}}(k+p\Delta t^*\mid k)$ is the same too. In the intra-day short time scale dispatch stage, for each time interval in the prediction horizon N, the energy stored in the battery and UC must satisfy the HESS's discrete-time difference dynamic formula, as illustrated by (28)-(29). The battery power at time $k+\Delta pt^*$ is represented by $P_{\text{bat}}^{i}(k+\Delta pt^*\mid k)$, calculated as $P_{\text{bat}}^{i}(k+p\Delta t^*\mid k)=P_{\text{bat}}^{i}(k)+\sum_{j=1}^{p}\Delta P_{\text{bat}}^{i}(k+j\Delta t^*\mid k)$, which indicates that the actual battery output is composed of the planned value and adjustment of intra-day, and positive value demonstrate the battery is in charging state, negative value is in discharging state. It is the same for UC. Charge and discharge efficiency of batteries and UC are also taken into account in (30). Equations (31) and (32) indicate that the stored energy in battery and UC during intra-day must be bounded by a predefined upper and lower bounds according to the actual status of HESS. This also reflects that the HESS must meet the constraints of remaining capacity when absorbing fluctuations. Equations (33) and (34) set up the limitation of discharging and charging power, which means that the actual power of HESS after adjustment cannot exceed the bound of power rating $\Delta P_{\text{bat}}^{i,\max}$, $\Delta P_{\text{bat}}^{\min}$, $\Delta P_{\text{uc}}^{\max}$, $\Delta P_{\text{uc}}^{\min}$ constrain the dynamic adjustment range of the battery and UC, these parameters constrain the ramp rate power of the battery and UC during the intra-day adjustment. The active power flowing through both side of the converter are restricted by their rated power capacities, as declared in (37) and (38).

V. Cade Study

In order to verify the effectiveness of the proposed energy management strategy, a busy HSR line in north-west China is considered for the case study. In the later part of this chapter, the optimization results of day-ahead and intra-day stage are given respectively, and the economics of system operation under different situations are compared and analyzed. A contrast between proposed intra-day rolling optimization and optimization without feedback is conducted.

A. Case Introduction and Parameters Description

Two neighbouring traction substations at different areas supplied by different utility grid was studied in this paper. The topology of the system is shown in Fig. 1. The PV converter with installed capacity 2MW, and historical solar irradiance can be obtained from [37]. The PV converter uses the maximum power point tracking to ensure power output. With regard to HESS, lithium batteries and UCs are used in substations. Optimal capacity configuration for batteries and UC is obtained from reference [34], All the main parameters of the HESS are presented in Table I. The time interval of day-ahead Δt =1min, rolling cycle of intra-day is 15s, and time horizon N=12. The schemes of electricity price implemented by state grid at different districts is also considered, including fixed price and time-of-use price. The unit price of electricity charge and demand charge are shown in Table II, the punishment charge price is equal to the exchange electricity price at district where

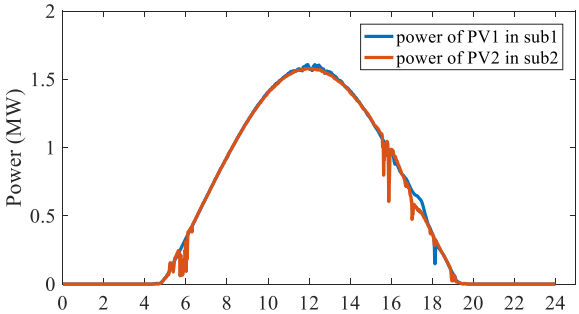

Fig. 5 The power profile for PV generation

traction substation is located. The PV output of day-ahead is shown in Fig. 5.

TABLE I
PARAMETERS OF HYBRID ENERGY STORAGE SYSTEM

Parameters	Battery	Ultracapacitor
Rated power(MW)	3	8
Rated Capacity(MWh)	5	0.45
Efficiency(charge/discharge)(%)	0.8	0.95
SOC minimum(%)	20	5
SOC maximum(%)	80	95
Initial SOC(%)	50	50
Self-discharge rate(%)	5	0

TABLE II
PARAMETERS OF THE ELECTRICITY CHARGE

Type of electricity charge			Dist1	Dist2
exchanged electricity charge	Valley(¥/kWh)	0:00-6:00 22:00-00:00	0.782	0.370
	Peak(¥/kWh)	8:00-11:00 18:00-21:00		1.252
	Intermediate (¥/kWh)	7:00-8:00 12:00-17:00		0.75
demand charge price(¥/kW)			1.2	1.6

B. Optimal scheduling results of day-ahead

At a day-ahead optimal stage, the goal is to minimize the operation cost of the railway system. The 2hours details of traction load process and operation curve of HESS are presented in Fig.6 (a)-(d). Fig. 6(a) show the optimized grid power of traction substation at district1 (abbreviated as sub1) between 8:00 and 10:00 period. In contrast, as the most basic case, the power of conventional traction substation without PV and HESS is also presented in Fig. 6(a). Power and SOC of HESS during these 2 hours are also drawn, as shown in Fig. 6(b). Form Fig. 6(a), the peak load power of traction substation integrated with PV and HESS has been shaved such as 8:00am and 10:00am, which contribute to reducing the demand charge. And the RB power is almost fully absorbed by HESS, which greatly reduce electric energy fed back to grid, avoiding paying penalty bills, at the same time, this part of energy is used to save exchange electricity charge. From Fig. 6(c), it is obvious that the peak power of sub2 has been shaved effectively. This is due to the high rate of RB, the RB energy absorbed by HESS, combined with the PV output, supply power at peak of substation load period. Moreover, the sub2 is at the peak of electricity price from 8:00 to 10:00, and the FREM system controls the HESS for more active charging and discharging. This also explain the remark decline of electricity cost in Table III. In Fig .6(d), the UC is frequently charged and discharged, while the running curve of battery is relatively stable, which also confirm battery responds to long-term energy needs while UC respond to severe power fluctuations. The optimized operation cost results of one day are listed in Table III.

As illustrated in Table III, the exchange electricity charge, demand charge and punishment charge of sub1 are reduced by 21.3%, 38.7% and 91%, respectively, compared to the basic case, total cost saving is 32.7%. The three types of charge of sub2 are reduced by 50%, 46.2% and 86.3% respectively, and total cost saving is 58%. Traction sub2 is located in the typical section of long-ramp, the ratio of RB is high. After access of HESS, the punishment charge for the traction sub2 was reduced from 25,169 to 3,455, indicating that 86% of the RB energy was recycled.

TABLE III
OPERATION COSTS BEFORE AND AFTER OPTIMIZATION

Substation	sub1		sub 2	
Price Scheme	Fixed price		TOU price	
	Without PV nor HESS	With PV and HESS	Without PV nor HESS	With PV and HESS
EC (¥)	66961	52370	55203	26972
DC (¥)	17370	10644	20522	11040
PC (¥)	10851	1030	25169	3455
Total Cost	95182	64044	100894	41467

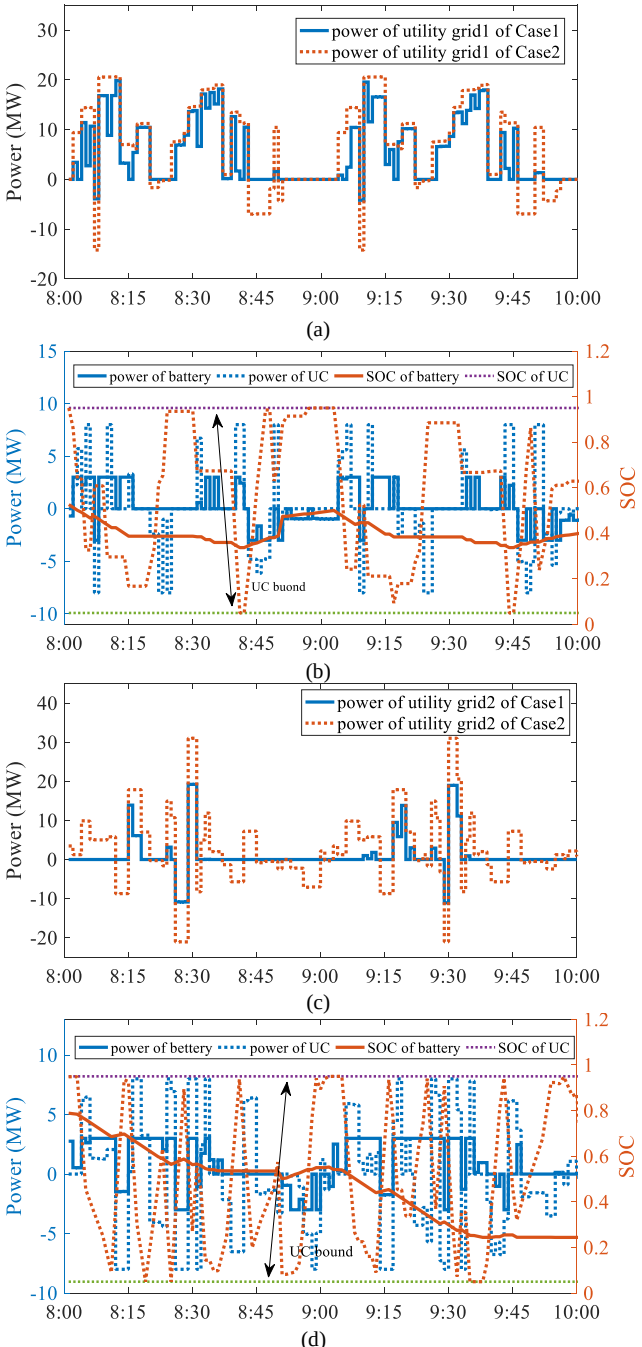

Fig. 6 Optimized result of sub at 8:00 to 10:00. (a) Power of sub1 with and without PV and HESS and PV output. (b) Charge and discharge of battery and UC and SOC of HESS. (c) Power of traction sub2 with and without PV and HESS and PV output. (d) Charge and discharge of battery and UC and SOC of HESS.

Taking sub1 as example, the different cases are compared for evaluating the system configuration and parameters impacts on economical operation of FTPSS, the result is given in Table IV. From Table IV, the most economical operation solution is case of both HESS and PV, the negative increase in case of only PV is due to the PV power feeding back to the grid, so it's necessary to actively reduce the PV output and adjust train operation strategy. Therefore, the installation of energy storage is reasonable. In case of only battery, the single battery can also achieve the cost reduction of 20%, but frequent charge and discharge will shorten the life. Comparing different electricity price schemes, the TOU price can better encourage HESS dispatch. Fig. 7 also shows that HESS is more actively dispatched to reduce the traction load at the peak of the grid.

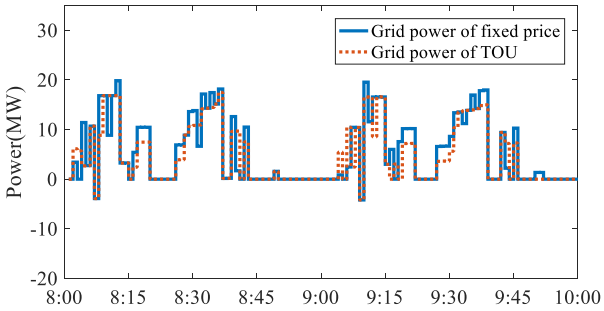

Fig. 7 HESS Comparison of different price schemes.

TABLE IV
COMPARISON OF DIFFERENT CASES

	Fixed price		TOU price	
	Total cost	Cost reduction	Total cost	Cost reduction
None of HESS and PV	95182	--	106200	--
Only PV	96206	-1.07%	107436	-1.16%
Only battery	76944	19.1%	84995	20%
Only HESS	72037	24.3%	78626	26%
Both HESS and PV	64044	32.7%	69814	34.3%

C. *Rolling feedback results of intra-day*

In the intra-day feedback correction stage, the fluctuations of traction load and PV output are taken into account, its objectives is to track the optimal inlet-line power and running curve of HESS. In general, high value of inlet-line power tracking weight result in better tracking performance, at the expense of the tracking of HESS SOC. As a trade-off, the weight factor of inlet-line in (26) is set as ω_p =300. To reduce the life loss caused by frequent adjustment of battery power, the supply-demand imbalance between source-load is compensated by UC first, the weight factor ω_{bat} is larger than ω_{uc}, thus ω_{bat} =600 and ω_{uc} =400 here. The set of control increment weight coefficients in objective function (26) can be found in [27]. In case of intra-day, the variance of the prediction error is set to 10%.

Taking sub1 as example, Fig. 8 illustrate the tracking effectiveness of proposed intra-day feedback control strategy. When the railway is actually running, the actual traction load and PV output of traction substation are different from the

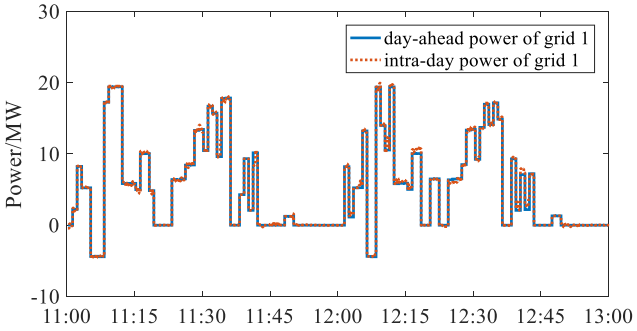

Fig. 8 Intra-day optimized grid power result of sub1.

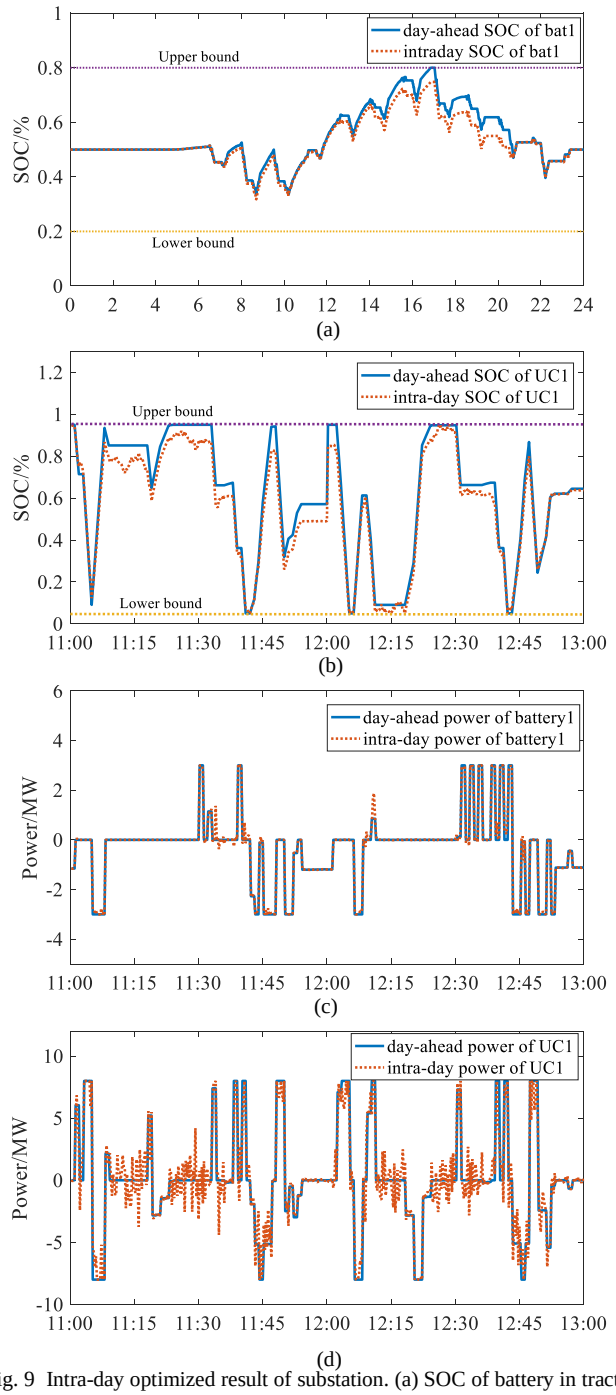

Fig. 9 Intra-day optimized result of substation. (a) SOC of battery in traction sub1. (b) SOC of UC in traction sub1. (c) Power of battery in traction sub1. (d)Power of UC in traction sub1

forecast values of day-ahead. If the FTPSS and HESS works based on the day ahead dispatching plan, all the measures to match the fluctuation is required to the main grid, with consequent strong fluctuation of the FTPSS power exchanged at grid-side. Fig. 8 is the result of intra-day based on MPC feedback correction. It is obvious that the proposed rolling feedback optimization has good performance on tracing utility grid power set in day-ahead. The power fluctuation result from PV and traction load uncertainty are smoothed by the adjustment of HESS. By intra-day optimization, the mismatch between the actual presumption realization and dispatch plan is compensated. At the same time, it avoids the additional fines charged by the grid operator due to the actual intraday dispatch of the substation deviation from the day-ahead plan reported [38].

Fig. 9 shows the one day SOC curve set in day-ahead and intra-day feedback control result of battery and 2hours SOC of UC. From Fig. 9(a) and (b), it is obvious that the SOC of battery and UC can generally track the plan of day-ahead. The difference of SOC curve between the intra-day and the day-ahead of the HESS is due to the FREM system controls the adjustment of the HESS to the day-ahead operation plan. Fig.9 (c) and (d) show that the comparison of the day-ahead and intra-day power of HESS, the battery output is rarely adjusted from 11:00 to 13:00, instead the power profile of the UC changes frequently. This shows that the FREM system dispatch the UC to respond to power fluctuations as well as ensure that the SOC of UC does not exceed the limit, and avoid excess life loss of battery result from frequent charge and discharge.

If the forecast of RES and load is 100% accurate, then it can be carried out and obtain the ideal cost of the day, the optimization result based on 100% accurate forecast is defined as ideal cost [25], [39]. Table V show the comparison of proposed day-ahead intra-day two stage rolling optimization method and ideal optimal cost for each substation. From Table V, it can be seen that after two stage optimization, the total cost of two traction substation is close to the ideal cost, where there is 2.3% and 6.3% of difference.

TABLE V
TWO-STAGE OPTIMIZATION RESULT AND IDEAL COST

	Sub1 ideal cost	Sub1 cost of case1	Sub2 ideal cost	Sub2 cost of case1
EC(¥)	53130	53308	27049	27834
DC(¥)	11192	12122	12241	12811
PC(¥)	996	1394	3487	4851
total cost(¥)	65318	66824	42777	45496

D. Comparison with scenario-based method

To illustrate the tracking effectiveness of proposed feedback control, in the case of proposed method and substation energy management based scenario method in [19] are compared. The scenario-based method determines uncertainty through scenario reduction technologies, and the constraints of power supply and demand balance are required to be satisfied in each retained scenario. However, at the stage of intra-day operation, this balance only exists in a few determinate scenarios, as a

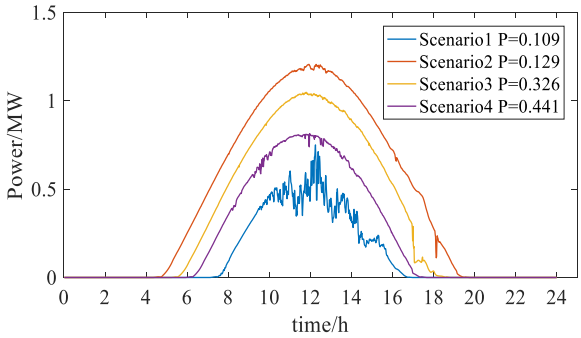

Fig. 10 Typical scenarios of PV generation after scenario reduction.

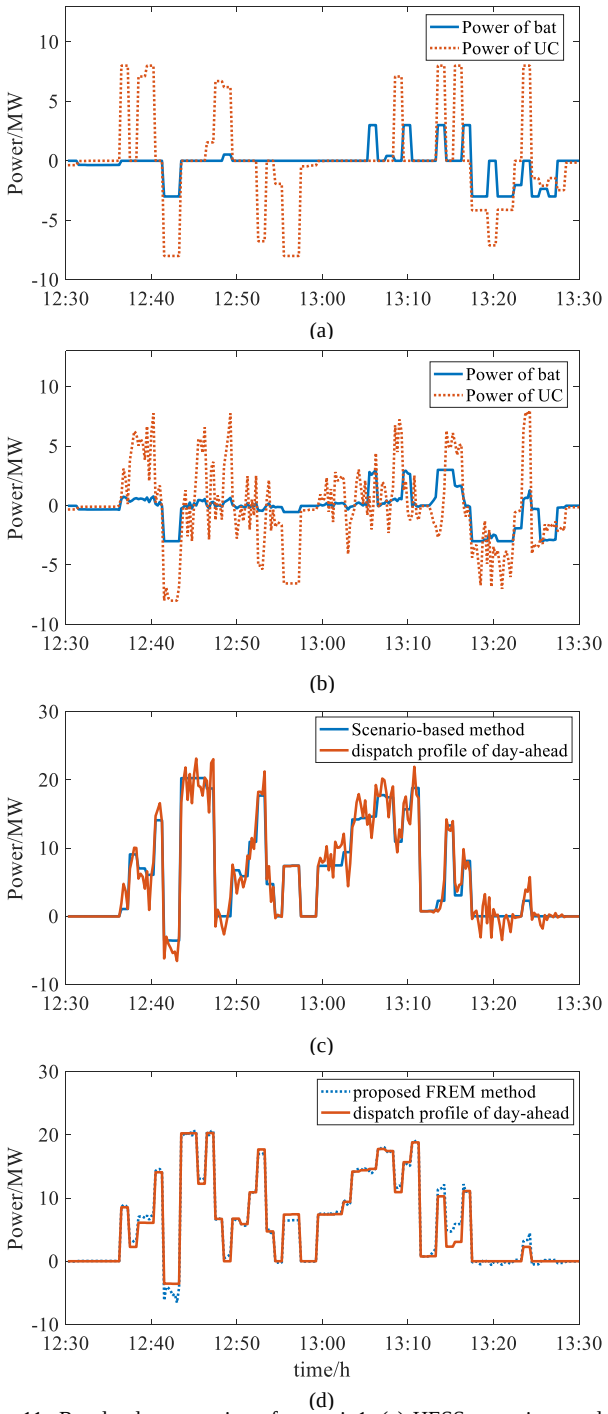

Fig. 11 Results demonstration of scenario1. (a) HESS operation results of scenario method (b) HESS operation results of FREM. (c) Utility grid power based on scenario method (d) Utility grid power based on FREM.

result of the forecast errors of PV output and traction load. If the operation scheme is carried out based on several special scenarios, the power fluctuations of the utility grid will be presented. Taking sub1 as example, the corresponding PV scenarios and probabilities are shown in Figure 10, and the comparison between the method proposed in this paper and for some time periods is shown in Fig 11 and Fig 12. The optimization results are summarized in Table VI.

TABLE VI
COMPARISON OF DIFFERENT CASES

	Scenario-based method	Proposed FREM
EC (¥)	54879	54019
DC (¥)	11984	12236
PC (¥)	3102	1834
Total Cost	69965	68089

It can be seen from Table VI that the energy management strategy proposed in this paper is slightly better than the scenario-based method in terms of economic performance. As shown in Fig. 11(c)-(d) and Fig. 12(c)-(d),the main advantages are reflected in the control of utility grid power fluctuation and the tracking of day-ahead plan. Although the scenario-based method considers the influence of uncertainty, and has some risk aversion ability, the kernel idea is still to use a large number of deterministic scenes to represent uncertainty. It can only ensure that the power and load are balanced separately in the few remaining scenes. The FREM proposed in this paper reduces the power fluctuation of utility grid by changing the HESS output plan during intra-day.

The average relative error (AVE) is defined as the average of the sum of the absolute value of the difference between the intra-day inlet-line power and the planned value of day-ahead, it is calculated as follow, where N is the number of data points:

$$\mathrm{AVE}=\frac{1}{N}\sum_{t=1}^{N}\frac{\left|P^{t}_{\mathrm{grid,intra}}-P^{t}_{\mathrm{grid,day\text{-}ahead}}\right|}{P^{t}_{\mathrm{grid,day-ahead}}} \tag{39}$$

Table VII shows the inlet-line power AVE of the four scenarios generated by the scenario-based method and the method proposed in this paper. As shown in Table VII, it is obvious that the proposed multi-time scale FREM performs better than the scenario-based method, the proposed method reduces the AVE of grid power by nearly 60% compared with the scenario method.

E. Performance analysis

Table VIII shows the single optimization average computation time with different prediction horizons. This method is implemented under the environment of MATLAB R2016 with the integration of YALMIP toolbox (version 20190425) and IBM ILOG CPLEX solver (version 12.9). The numerical simulation is performed on a computer with Intel

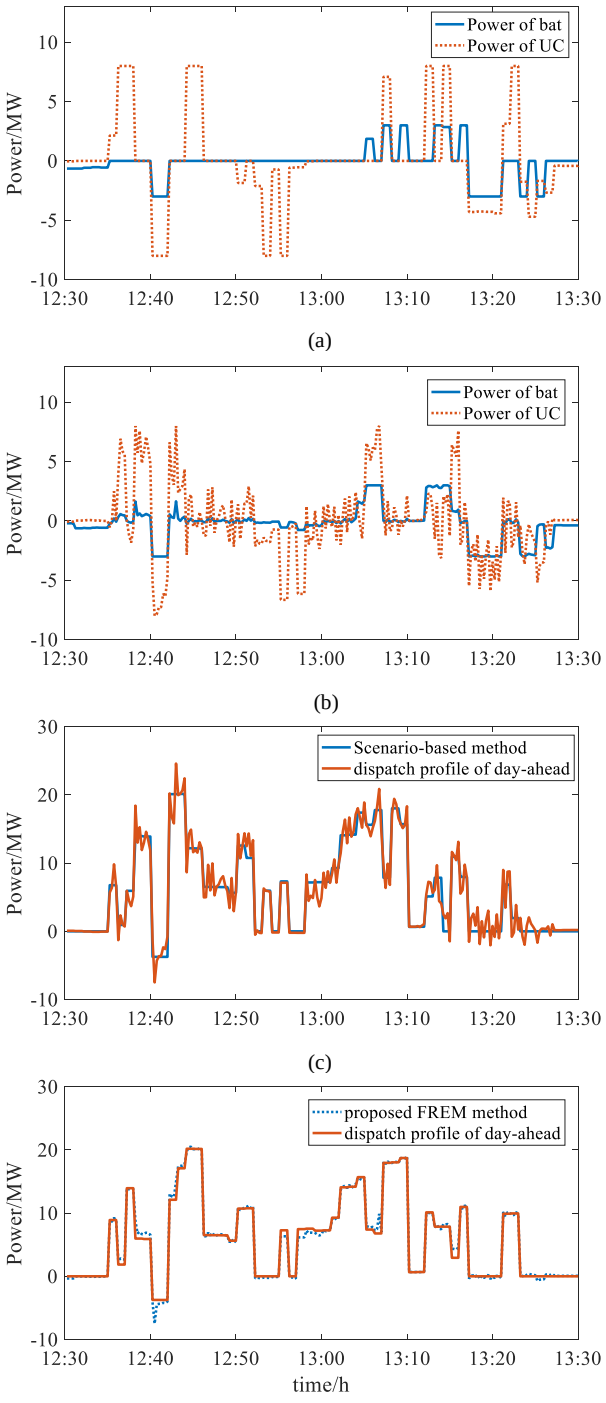

Fig. 12 Results demonstration of scenario4. (a) HESS operation results of scenario method (b) HESS operation results of FREM. (c) Utility grid power based on scenario method (d) Utility grid power based on FREM.

TABLE VII
AVE OF COMPARATIVE CASES

	Scenario1		Scenario2		Scenario3		Scenario4	
	Scenario-based	Proposed FREM	Scenario-based	Proposed FREM	Scenario-based	Proposed FREM	Scenario-based	Proposed FREM
AVE(%)	17.61	6.37	20.16	8.37	18.84	7.47	18.55	7.25

Core I5-8300 CPU at 2.3 GHz and 16 GB RAM. It can be seen from Table VIII present that as the prediction time horizon increases, the computation time also increases. Since the computation time is shorter than the corresponding time interval, intra-day optimization ensures that the results are obtained before the next upcoming time interval. As a result, the computation time is sufficient for the short-term operation of railway.

TABLE VIII
COMPUTATIONAL PERFORMANCE

Prediction horizon N	Computation time(s)	
	Day-ahead	Intra-day
1	13.23	0.75
4		0.854
12		0.982
60		1.449
120		1.7108
240		2.7836

VI. CONCLUSION

A FREM system and its operation strategy are proposed and verified in this paper. The energy management strategy is divided into two parts: day-ahead economic dispatch and intra-day rolling feedback correction. The day-ahead dispatch optimization guarantees the economic operation of railway system, and MPC-based intra-day rolling feedback control is implemented to compensate the power fluctuation result from PV and traction load forecast error. The case study shows that the integration of HESS and PV generation reduces the total operation cost of FTPSS by 32.7%. In the typical long-ramp section where traction substation 2 is located, 86.3% of RB power is effectively used. The study show that compared with the scenario-based method, the proposed control strategy can ensure the economy operation while handling uncertainties of RES and traction load effectively. Under the worst-case scenario, the average relative error of the inlet-line power of the traction substation is 8.37%, which is reduced by 60% compared with the case of scenario-based method. The computation time of a single intra-day optimization is less than 5 seconds, indicating that the proposed strategy can be used as a reference for the short-term operation of railway. On the basis of the field application, the real-time optimization is worthy of further study and the research results will be summarized and published.

REFERENCES

[1] Q. Wang, J. Lu, Q. Wang, and J. Duan, "Transient overvoltage study of auto-passing neutral section in high-speed railway," in *2017 IEEE Transportation Electrification Conference and Expo, Asia-Pacific (ITEC Asia-Pacific)*, 2017, pp. 1–5.

[2] Y. Chen, M. Chen, Z. Tian, Y. Liu, and S. Hillmansen, "VU limit pre-assessment for high-speed railway considering a grid connection scheme," *Iet Gener. Transm. Distrib.*, vol. 13, no. 7, pp. 1121–1131, 2019.

[3] S. Östlund, "Rail power supplies going more power electronic [technology leaders]," *IEEE Electrification Mag.*, vol. 2, no. 3, pp. 4–60, 2014.

[4] E. P. de la Fuente, S. K. Mazumder, and I. G. Franco, "Railway Electrical Smart Grids: An introduction to next-generation railway power systems and their operation.," *IEEE Electrification Mag.*, vol. 2, no. 3, pp. 49–55, 2014.

[5] I. Krastev, P. Tricoli, S. Hillmansen, and M. Chen, "Future of electric railways: advanced electrification systems with static converters for ac railways," *IEEE Electrification Mag.*, vol. 4, no. 3, pp. 6–14, 2016.

[6] X. He, A. Guo, X. Peng, Y. Zhou, Z. Shi, and Z. Shu, "A traction three-phase to single-phase cascade converter substation in an advanced traction power supply system," *Energies*, vol. 8, no. 9, pp. 9915–9929, 2015.

[7] E. Pilo, S. K. Mazumder, and I. González-Franco, "Smart electrical infrastructure for AC-fed railways with neutral zones," *IEEE Trans. Intell. Transp. Syst.*, vol. 16, no. 2, pp. 642–652, 2014.

[8] X. He *et al.*, "Advanced cophase traction power supply system based on three-phase to single-phase converter," *IEEE Trans. Power Electron.*, vol. 29, no. 10, pp. 5323–5333, 2013.

[9] X. He, P. Han, M. Zhu, S. Gao, and W. Peng, "Advanced Traction Power Supply System Based on Modular Multilevel Converters," in *2018 Asian Conference on Energy, Power and Transportation Electrification (ACEPT)*, pp. 1–8.

[10] L. Li, M. Wu, S. Wu, J. Li, and K. Song, "A Three-Phase to Single-Phase AC-DC-AC Topology Based on Multi-Converter in AC Electric Railway Application," *IEEE Access*, vol. 7, pp. 111539–111558, 2019.

[11] X. He *et al.*, "Power Flow Analysis of the Advanced Co-Phase Traction Power Supply System," *Energies*, vol. 12, no. 4, p. 754, 2019.

[12] P. Han *et al.*, "Fault Diagnosis and System Reconfiguration Strategy of Single-phase Three Level Neutral-Point-Clamped Cascaded Inverter," *IEEE Trans. Ind. Appl.*, 2019.

[13] S. D'Arco, L. Piegari, and P. Tricoli, "Comparative Analysis of Topologies to Integrate Photovoltaic Sources in the Feeder Stations of AC Railways," *IEEE Trans. Transp. Electrification*, vol. 4, no. 4, pp. 951–960, 2018.

[14] D. Serrano-Jiménez, L. Abrahamsson, S. Castaño-Solís, and J. Sanz-Feito, "Electrical railway power supply systems: Current situation and future trends," *Int. J. Electr. Power Energy Syst.*, vol. 92, pp. 181–192, 2017.

[15] S. Khayyam, F. Ponci, J. Goikoetxea, V. Recagno, V. Bagliano, and A. Monti, "Railway energy management system: Centralized–decentralized automation architecture," *IEEE Trans. Smart Grid*, vol. 7, no. 2, pp. 1164–1175, 2015.

[16] S. Khayyam, N. Berr, L. Razik, M. Fleck, F. Ponci, and A. Monti, "Railway system energy management optimization demonstrated at offline and online case studies," *IEEE Trans. Intell. Transp. Syst.*, vol. 19, no. 11, pp. 3570–3583, 2018.

[17] L. Razik, N. Berr, S. Khayyam, F. Ponci, and A. Monti, "REM-S–Railway Energy Management in Real Rail Operation," *IEEE Trans. Veh. Technol.*, vol. 68, no. 2, pp. 1266–1277, 2018.

[18] J. A. Aguado, A. J. S. Racero, and S. de la Torre, "Optimal operation of electric railways with renewable energy and electric storage systems," *IEEE Trans. Smart Grid*, vol. 9, no. 2, pp. 993–1001, 2016.

[19] İ. Şengör, H. C. Kılıçkıran, H. Akdemir, B. Kekezoğlu, O. Erdinc, and J. P. Catalao, "Energy management of a smart railway station considering regenerative braking and stochastic behaviour of ESS and PV generation," *IEEE Trans. Sustain. Energy*, vol. 9, no. 3, pp. 1041–1050, 2017.

[20] C. F. Calvillo, Á. Sánchez-Miralles, and J. Villar, "Synergies of electric urban transport systems and distributed energy resources in smart cities," *IEEE Trans. Intell. Transp. Syst.*, vol. 19, no. 8, pp. 2445–2453, 2017.

[21] Y. Sun, Z. Li, M. Shahidehpour, and B. Ai, "Battery-based energy storage transportation for enhancing power system economics and security," *IEEE Trans. Smart Grid*, vol. 6, no. 5, pp. 2395–2402, 2015.

[22] A. Di Giorgio, F. Liberati, A. Lanna, A. Pietrabissa, and F. D. Priscoli, "Model predictive control of energy storage systems for power tracking and shaving in distribution grids," *IEEE Trans. Sustain. Energy*, vol. 8, no. 2, pp. 496–504, 2016.

[23] J. Sachs and O. Sawodny, "A Two-Stage Model Predictive Control Strategy for Economic Diesel-PV-Battery Island Microgrid Operation in Rural Areas," *IEEE Trans. Sustain. Energy*, vol. 7, no. 3, pp. 903–913, 2016.

[24] W. Gu, Z. Wang, Z. Wu, Z. Luo, Y. Tang, and J. Wang, "An online optimal dispatch schedule for CCHP microgrids based on model predictive control," *IEEE Trans. Smart Grid*, vol. 8, no. 5, pp. 2332–2342, 2016.

[25] F. Garcia-Torres, C. Bordons, and M. A. Ridao, "Optimal economic schedule for a network of microgrids with hybrid energy storage system using distributed model predictive control," *IEEE Trans. Ind. Electron.*, vol. 66, no. 3, pp. 1919–1929, 2018.

[26] F. Garcia-Torres and C. Bordons, "Optimal economical schedule of hydrogen-based microgrids with hybrid storage using model predictive control," *IEEE Trans. Ind. Electron.*, vol. 62, no. 8, pp. 5195–5207, 2015.
[27] F. Garcia-Torres, L. Valverde, and C. Bordons, "Optimal load sharing of hydrogen-based microgrids with hybrid storage using model-predictive control," *IEEE Trans. Ind. Electron.*, vol. 63, no. 8, pp. 4919–4928, 2016.
[28] S. Li, B. De Schutter, L. Yang, and Z. Gao, "Robust model predictive control for train regulation in underground railway transportation," *IEEE Trans. Control Syst. Technol.*, vol. 24, no. 3, pp. 1075–1083, 2015.
[29] H. Novak, V. Lešić, and M. Vašak, "Hierarchical coordination of trains and traction substation storages for energy cost optimization," in *2017 IEEE 20th International Conference on Intelligent Transportation Systems (ITSC)*, 2017, pp. 1–6.
[30] H. Novak, M. Vašak, and V. Lešić, "Hierarchical energy management of multi-train railway transport system with energy storages," in *2016 IEEE International Conference on Intelligent Rail Transportation (ICIRT)*, 2016, pp. 130–138.
[31] H. Novak, V. Lešić, and M. Vašak, "Hierarchical Model Predictive Control for Coordinated Electric Railway Traction System Energy Management," *IEEE Trans. Intell. Transp. Syst.*, 2018.
[32] Y. Zhang, R. Wang, T. Zhang, Y. Liu, and B. Guo, "Model predictive control-based operation management for a residential microgrid with considering forecast uncertainties and demand response strategies," *IET Gener. Transm. Distrib.*, vol. 10, no. 10, pp. 2367–2378, 2016.
[33] W. El-Baz, P. Tzscheutschler, and U. Wagner, "Day-ahead probabilistic PV generation forecast for buildings energy management systems," *Sol. Energy*, vol. 171, pp. 478–490, 2018.
[34] Y. Liu, M. Chen, S. Lu, Y. Chen, and Q. Li, "Optimized Sizing and Scheduling of Hybrid Energy Storage Systems for High-Speed Railway Traction Substations," *Energies*, vol. 11, no. 9, p. 2199, 2018.
[35] X. Yan, D. Abbes, and B. Francois, "Uncertainty analysis for day ahead power reserve quantification in an urban microgrid including PV generators," *Renew. Energy*, vol. 106, pp. 288–297, 2017.
[36] S. Yang, K. Song, and G. Zhu, "Stochastic Process and Simulation of Traction Load for High Speed Railways," *IEEE Access*, vol. 7, pp. 76049–76060, 2019.
[37] N. MIDC, "National Renewable Energy Laboratory Measurement and Instrumentation Data Center (NREL MIDC) Solar Position and Intensity (SOLPOS) Calculator," *Online Httpwww Nrel Govmidcsolpossolpos Html*, 2010.
[38] F. Sossan, E. Namor, R. Cherkaoui, and M. Paolone, "Achieving the dispatchability of distribution feeders through prosumers data driven forecasting and model predictive control of electrochemical storage," *IEEE Trans. Sustain. Energy*, vol. 7, no. 4, pp. 1762–1777, 2016.
[39] Z. Wu, X.-P. Zhang, J. Brandt, S.-Y. Zhou, and L. Jia-Ning, "Three control approaches for optimized energy flow with home energy management system," *IEEE Power Energy Technol. Syst. J.*, vol. 2, no. 1, pp. 21–31, 2015.

Minwu Chen (M'17) received the B.Eng. and Ph.D. degrees in electrical engineering from Southwest Jiaotong University, Chengdu, China, in 2004 and 2009, respectively.
From 2010 to 2012, he undertook postdoctoral researches in the China Railway First Survey and Design Institute Group, Xi'an, China. Since 2018, he has been a Full Professor at the School of Electrical Engineering, Southwest Jiaotong University, Chengdu, China. From 2014 to 2015, he was a Visiting Scholar at the University of Birmingham, Birmingham, UK. His research interests include new technology and power quality for railway traction systems.

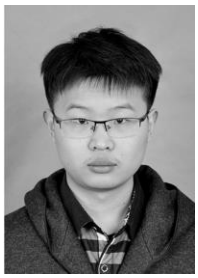

Zhe Cheng received the B.Eng. degree in smart grid information engineering from Qingdao University of Science and Technology, Qingdao, China, in 2017, He is currently working toward the M.Eng. degree in electrical engineering from Southwest Jiaotong University, Chengdu, China. His current research interest is the energy management of electric railway system integrated energy storage and renewable energy.

Yuanli Liu received the B.Eng. degree in electrical engineering from Southwest Jiaotong University, Chengdu, China, in 2017, where he is currently working toward the M.Eng. degree in the School of Electrical engineering, Southwest Jiaotong University. His primary research interests is the optimal operation and planning for the integration of renewable energy and storage in electric railway system.

Yilin Cheng received the B.Eng. degree in electrical engineering from Southwest Jiaotong University, China, in 2017, where he is currently working toward the M.Eng. degree in electrical engineering. His research interests include railway power traction systems, energy storage systems and converter control.

Zhongbei Tian received the B.Eng. degree from Huazhong University of Science and Technology, Wuhan, China, in 2013, and the B.Eng. and Ph.D. degrees in electrical and electronic engineering from the University of Birmingham, Birmingham, UK, in 2013 and 2017, respectively. He is currently a Research Fellow with the University of Birmingham. His research interests include railway traction systems and power network modeling, energy systems optimization, advanced power systems design, and the analysis of electric railways.